



# Enhancing response characteristics of palladium-doped vanadium pentoxide on a porous silicon substrate as gas sensor synthesized by pulsed laser deposition

Mayada A. Abed<sup>1</sup> · Falah A.-H. Mutlak<sup>1</sup>

Received: 9 September 2023 / Accepted: 2 November 2023 / Published online: 14 December 2023  
© The Author(s), under exclusive licence to Springer Science+Business Media, LLC, part of Springer Nature 2023

## Abstract

A gas sensor utilizing  $V_2O_5/Pd$  thin films has been successfully created by pulse laser deposition on porous silicon substrate, demonstrating rapid response times and superior sensitivity for detecting gases at low temperatures. The investigation of sensor response, selectivity, and stability demonstrates the impressive sensing capabilities of the thin films. Vanadium pentoxide films doped with palladium ( $V_2O_5/Pd$ ) are fabricated through pulsed laser deposition technique, with varying laser pulse energy (600, 800, and 1000) mJ/pulse, for the purpose of sensing applications related to Hydrogen Sulfide ( $H_2S$ ) and Nitrogen Dioxide ( $NO_2$ ). The ablation procedure entails the utilization of a Q-switched Nd:YAG laser that operates at a specific wavelength of 1064 nm. The laser system exhibits pulse duration of 10 ns and a repetition rate of 1 Hz when operating on a porous silicon n-type Si (111) substrate. The X-ray diffraction, UV–Vis Spectroscopy, Raman scattering, Photoluminescence spectroscopy, and field emission-scanning electron microscopy techniques were employed to investigate the crystal structure, optical structure, and morphological properties of the  $V_2O_5/Pd$  NPs. As the energy of the pulse laser grows, the presence of well-defined peaks in the  $V_2O_5/Pd$  thin film indicates an enhancement in its crystal-line structure. The size of the surface grains exhibit an augmentation, accompanied by an increase in the energy gap, leading to an elevated level of homogeneity. This study aimed to evaluate the influence of Pd on the development kinetics of vanadium pentoxide nanoparticles. The findings of this investigation demonstrated that the addition of Pd resulted in several notable effects, including improved sensitivity, reduced operational temperature requirements, and the capacity to maintain high sensitivity levels even at room temperature.

**Keywords** Vanadium pentoxide · Palladium · Pulse laser deposition · Gas sensor · Porous silicon · Hydrogen sulfide · Nitrogen dioxide

---

✉ Falah A.-H. Mutlak  
Falah.mutlak@sc.uobaghdad.edu.iq

Mayada A. Abed  
basmayadt6799@gmail.com

<sup>1</sup> Department of Physics-College of Science, University of Baghdad, Baghdad, Iraq

## 1 Introduction

Vanadium (V) is a widely recognized transition metal that has the ability to generate various oxides. The primary oxides of vanadium consist of vanadium monoxide (VO, exhibiting a violet colour), vanadium sesquioxide ( $V_2O_3$ , displaying a green colour), vanadium dioxide ( $VO_2$ , characterized by a blue colour), and vanadium pentoxide ( $V_2O_5$ , presenting a yellow colour) (Le et al. 2019; Mane et al. 2019). Among several phases, vanadium pentoxide ( $V_2O_5$ ) is considered to be the thermodynamically most stable oxide. Additionally,  $V_2O_5$  is known to occur in multiple polymorphs.  $V_2O_5$  exhibits a notable prevalence in natural occurrences, rendering it exceedingly plentiful. Moreover, this compound is characterized by its relatively low cost, making it economically accessible. Additionally,  $V_2O_5$  exhibits many oxidation states, specifically 7 and 8 (Laubach et al. 2007; Rathika et al. 2020; Hou et al. 2020).  $V_2O_5$  has been utilized in various applications, including water splitting, field effect transistors, supercapacitors, IR detectors, photodetectors, UV sensors, optical sensors, amperometric gas sensors, potentiometric sensors, electrochemical sensors, cataluminescence sensors, resistance gas sensors, gasochromic sensors, and humidity sensors, owing to its relatively open layered structure and unique properties (Slewa et al. 2020; Abd-Alghafour et al. 2017; Alam et al. 2020; Singh et al. 2018; Rajesh and Santhanalakshmi 2017; Aawani et al. 2019). Nanostructured  $V_2O_5$  materials exhibit distinct electrical and chemical characteristics in comparison to bulk  $V_2O_5$ . Their ultrafine dimensions result in a significantly increased surface area, hence rendering them highly advantageous for sensing investigations (Gross et al. 2018; Harb and Mutlak 2022a). Gas sensors have gained significant popularity in several fields due to their ability to detect toxic, dangerous, explosive, and greenhouse gases and vapours. There is a wide range of gas sensors. Resistive-based gas sensors employing metal oxides have gained significant popularity as the predominant gas sensing technology. This can be attributed to its distinctive characteristics, including cost-effectiveness, heightened sensitivity, high stability, rapid response time, and straightforward manufacturing and operational processes (Yıldırım et al. 2019; Amiri et al. 2020; Mirzaei et al. 2016; Mounasamy et al. 2020; Jwied et al. 2021a; Khudiar et al. 2021; Ahmed et al. 2022). Porous silicon (PS) possesses desirable attributes for the purpose of sensing investigations, primarily owing to its capacity to provide a substantial surface area and a porous configuration. Additionally, a chemical etching procedure can quickly fabricate it (Kh Hammad et al. 2023; Alber and Mutlak 1477, 2022; Jwied et al. 2021a; Mutlak 2014; Harb and Mutlak 2021; Ahmed et al. 2021; Abood and Mutlak 2020; Jwar et al. 2023). Hence, using composites comprising  $V_2O_5$  and PS holds significant potential for conducting gas sensing investigations (Ozdemir and Gole 2007). Prior research has established the capacity of dopants to function as catalysts or surface sites for gas absorption, hence augmenting the efficacy of the sensing mechanism. Therefore, the facilitation of the interaction between the film and the target gas was achieved through catalysis. The effectiveness of the active sites present in the film was improved by the inclusion of specific metal additives, notably Pd, Ag, and Pt, as evidenced in the cited references (Fardindoost and Irajizad A, Rahimi F, Ghasempour R. 2010; Naseri et al. 2013; Jolly Bose et al. 2016). Several approaches have been employed in the fabrication of  $V_2O_5$  thin films, including vacuum evaporation (Lu et al. 2000), sputter coating (West et al. 1992), thermal oxidation (Kei et al. 1992), sol-gel (Matthe et al. 2018), spray pyrolysis (Bouzidi et al. 2002), and pulsed laser deposition (Shaikshavali et al. 2019; Eric et al. 2020). Pulsed laser deposition (PLD) is a fundamental physical deposition technique utilized to produce thin films that may be applied to various substrates. PLD has numerous

benefits over alternative techniques, including one-step production, simple operation, rapid reactive processes, absence of component differences, and production of high-quality films at lower substrate temperatures (Julien et al. 1999). In reality, the drop in deposition temperature in the PLD process is compensated by the high energy of the ablated fragments in the laser-generated plasma plume. This versatile technique provides controllable thickness, stoichiometry, and composition, making it an excellent method for synthesizing thin films with superior structural and optical properties (Huotari et al. 2012). Deposition parameters such as laser energy, target-substrate separation, substrate temperature, and relative oxygen pressure affect PLD-grown V<sub>2</sub>O<sub>5</sub> thin coatings (Huotari et al. 2013). The target material is regularly ablated using a pulsed laser, typically at ultraviolet (UV) wavelengths within a high vacuum environment (Mutlak et al. 2021, 2017; Rashid et al. 2021a, b; Jwied et al. 2021b; Abed et al. 2021; Yousef and Ahmed 2021; Ahmed et al. 2018; Aswad et al. 1795). In most reports, the operating temperature is too high, with much longer response and recovery times (Birajdar and Adhyapak 2020). In this study, gas sensors utilizing a composite material of V<sub>2</sub>O<sub>5</sub> and Pd were generated through the procedure of PLD on porous silicon substrates. The primary objective was to decrease the operating temperature of the sensor while simultaneously reducing the response and recovery time. Furthermore, the sensor's extensive operational range in relation to gas concentration is also highly desirable. The synthesized target was subjected to examination in order to analyse its crystallinity, optical, and surface morphology properties. The investigations were conducted using X-ray diffraction (XRD), ultraviolet–visible (UV–Vis) spectroscopy, photoluminescence (PL), Raman spectroscopy, and field emission scanning electron microscopy (FESEM).

## 2 Experimental details

The V<sub>2</sub>O<sub>5</sub> and Pd powders, with a high purity of 99.9%, were acquired from Sigma Aldrich. These powders were then subjected to compression utilizing hydraulic type (SPE CAC) masking pellets. The powders were pressed by a 15 Tons hydraulic compressor for 3 min into a pellet. The hydraulic compressor's mold was washed with hydrochloric acid (HCl) and deionized water. The resulting target had a diameter of 3 cm. The primary objective of this endeavor should be to attain a significant level of thickness and uniformity in order to ensure the production of a deposit that is of high quality. The target synthesis process consists of three main steps. Photo-electrochemical etching (PECE) is a procedure characterized by the deliberate elimination of material from a surface through the synergistic influence of light and electrochemical processes (Mutlak and Taha 2017). The used n-type (111) Si wafer had a thickness of (600 ± 25) μm, resistivity of (0.1–100) ohm.cm, and was sliced into (1.5 × 1.5) cm<sup>2</sup> sections. Following this, the fragments underwent a process of air drying, followed by purification utilizing a solution consisting of hydrofluoric acid (HF) and ethanol at a ratio of 2:1. Furthermore, the provided sample was subjected to etching utilizing a diode laser with a wavelength of 532 nm, a current density of 20 mA/cm<sup>2</sup>, and an etching period of 12 min. The experiment was carried out using an electrolyte solution consisting of 48% hydrofluoric acid and 99.9% ethanol. Teflon cells, which are renowned for their high resistance to hydrofluoric acid (HF), have the capability to induce anodization etching. Following this, the utilization of Nd: YAG pulsed laser deposition (PLD) is implemented for the production of V<sub>2</sub>O<sub>5</sub>/Pd nanoparticles. The objects underwent laser ablation at laser strengths of 600 mJ/pulse, 800 mJ/pulse, and 1000 mJ/pulse, employing a laser wavelength of 1064 nm. A total of 300 shots were provided to the targets composed

of porous silicon with an n-type doping. The shots were delivered at a repetition rate of 1 Hz. Subsequently, the targets were subjected to a secondary ablation procedure utilizing a palladium (Pd) plate via PLD; ensuring uniform energy levels were maintained for all targets. The present study investigated the deposition of a  $V_2O_5$ /Pd thin layer on PS substrate using pulsed laser deposition. The substrate was porous silicon, which was placed inside the pulsed laser deposition system and maintained at a  $5 \times 10^{-2}$  mbar vacuum pressure. The separation between the  $V_2O_5$ , Pd pellets, and the substrate was 12 cm. The target was then ablated using a Q-switched Nd:YAG pulsed laser with the following parameters: 1064 nm wavelength, 10 ns pulse duration, and 1 Hz repetition rate. The laser energy was varied from 600 to 1000 mJ/pulse for 300 laser pulses to achieve sufficient laser fluence, estimated at 1.5 mm spot size using a 120 mm focal length planoconvex lens focused on the  $V_2O_5$  and Pd targets. The incident angle of the laser beam onto the  $V_2O_5$  and Pd targets was fixed at  $45^\circ$ . The  $V_2O_5$ /Pd thin film deposition occurred at room temperature. The schematic diagram for depositing the  $V_2O_5$ /Pd layer on the porous silicon substrate is depicted in Fig. 1.

The implementation of this methodology led to the synthesis of  $V_2O_5$ /Pd. The X-ray diffraction measurements were performed utilizing a Philips PW 1050 X-ray diffractometer with reference to JCPDS card No. 96-90-2222. The value of  $Cu\text{-}k\alpha$  is determined to be 1.54 Å. The UV-Vis spectrophotometer, the Shimadzu 1800 model from Japan, is employed for the purpose of quantifying the transmittance and absorption characteristics of  $V_2O_5$ /Pd. The emission spectra of photoluminescence within the wavelength range of 400–700 nm were measured using a fluorescence spectrophotometer. The Raman microscopy technique was employed in order to analyze and investigate the vibrational spectra

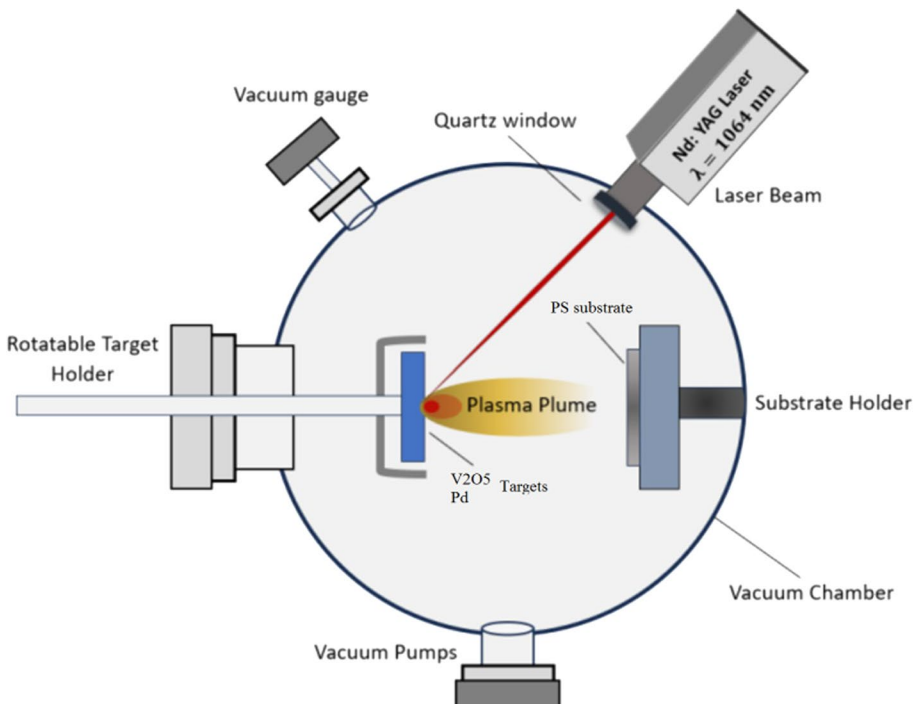
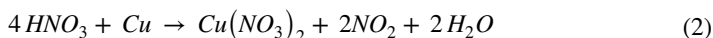
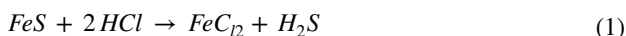


**Fig. 1** A schematic illustration experimental setup for the pulse laser deposition system

of the  $V_2O_5/Pd$  target and thin layers within the frequency range spanning from 100 to  $3500\text{ cm}^{-1}$ . When conducting gas sensing measurements, various aspects are taken into account, such as the sensitivity of the gas sensor detector, the response time, the recovery time, and a bias voltage of 6 V. Furthermore, the laboratory produced  $H_2S$  and  $NO_2$  gases. In the case of  $H_2S$ , a commonly employed method in laboratory settings is the use of a Büchner flask to treat ferrous sulfide with a potent acid. On the other hand, the production of  $NO_2$  is achieved through the reduction of concentrated nitric acid using a metal, such as copper.



The temperature range of the samples exhibited fluctuations ranging from 30 to  $250\text{ }^\circ\text{C}$ . The masks underwent vacuum evaporation using an Edward coating machine type 306, with porous silicon substrates serving as the underlying material. The mask employed in this work consists of aluminum foil with aluminum electrodes with a thickness of 300 nm. The spacing between each electrode is precisely 0.5 mm. The investigation involved manipulating the temperature of the samples within the range of  $30\text{ }^\circ\text{C}$  to  $250\text{ }^\circ\text{C}$  in order to assess the sensitivity, response time, and recovery time of the specimen. The experiment involved the use of a blend of 3%  $H_2S$  or  $NO_2$  and 97% air, with the concurrent application of a bias voltage of 6 V. The tests were performed for atmospheric air as well as for gases such as hydrogen sulfide ( $H_2S$ ) and nitrogen dioxide ( $NO_2$ ). The true sensitivity is obtained by feeding the mixed gas through a conduit over the sensor within the test chamber. The following is to test the gas sensor device: The gas is examined under a volumetric concentration of 50 ppm gas-to-air ratio, and needle valves are utilized to regulate the gas flow.

### 3 Results and discussion

#### 3.1 Microstructure characterizations

Thin films of vanadium pentoxide and palladium ( $V_2O_5/Pd$ ) were effectively produced on porous silicon (PS) films grown on n-type silicon (100) substrates using the pulsed laser deposition (PLD) process. Figure 2 presents an analysis of an X-ray diffraction (XRD) study on thin films of ( $V_2O_5/Pd$ ) at varying laser energy levels. The  $2\theta$  readings demonstrate a significant degree of agreement with the recognized standard (Reference: JCPDS No. 041–1426). The user has presented a series of numerical values, including (200), (001), (101), and (111).

Moreover, there are four diffraction peaks at  $2\theta = 16^\circ$ ,  $20^\circ$ ,  $21^\circ$ , and  $34^\circ$ , which align with the (200), (001), (101), and (111) crystal planes, respectively. The primary peak corresponding to the (111) plane of the orthorhombic  $V_2O_5$  phase was observed at an angle of 34 degrees.

According to the results obtained from the study conducted by PS, it is apparent that the peak observed at an angle of  $28.28^\circ$  exhibits distinct peaks corresponding to the (111) crystallographic orientation. We have tried to clarify in the XRD other peaks via cutting the peak of the PS as shown in Fig. 2a, b. The observation indicates the occurrence of Pd at its maximum intensity, observed at an angle of  $40.5^\circ$  ( $2\theta$ ), corresponding to the (111)

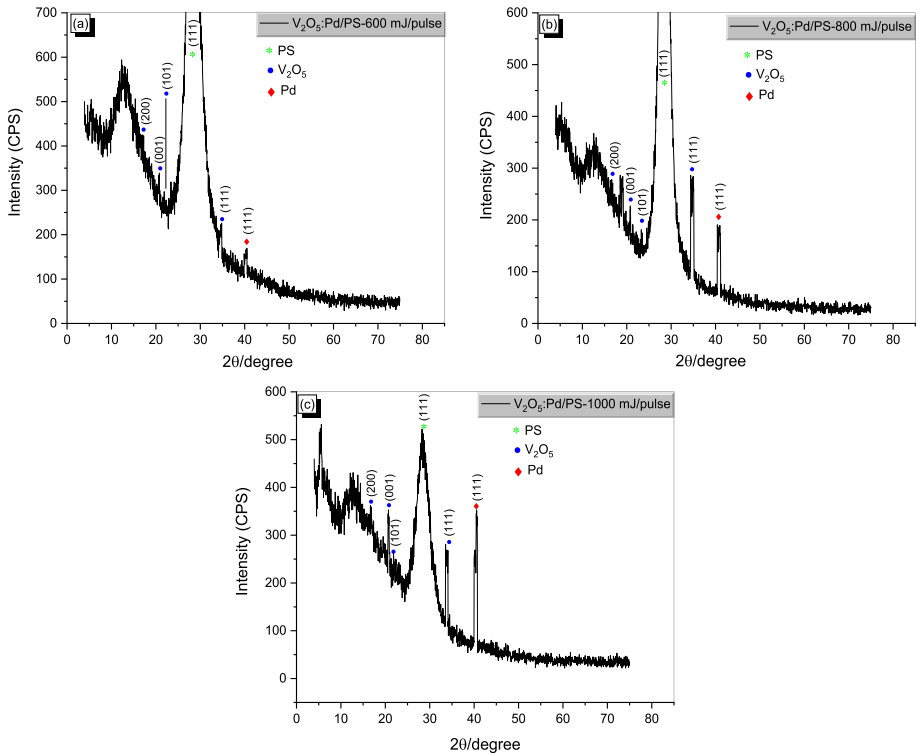


**Fig. 2** X-ray diffraction patterns for  $V_2O_5/Pd$  thin film using an Nd: YAG laser at 1064 nm with different laser deposited energy **a** 600 mJ/pulse, **b** 800 mJ/pulse, and **c** 1000 mJ/pulse

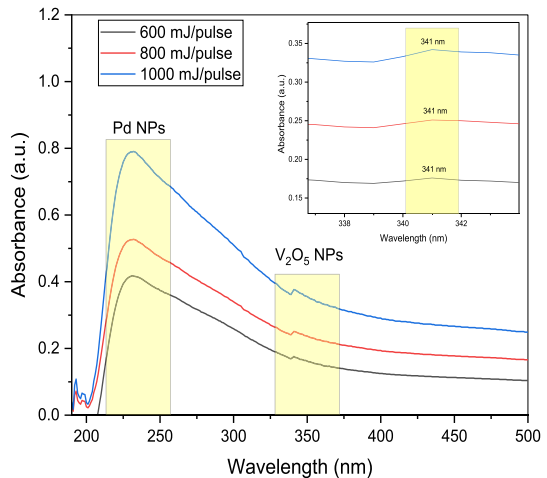
crystallographic lattice planes. The diffraction peak seen in the experiment may be precisely correlated with the crystal structure of face-centered cubic (fcc) Pd, as evidenced by the (JCPDS card No. 05–0681). The results suggest that the laser parameters can be adjusted in order to manipulate the size and structure of the particles. The X-ray diffraction (XRD) peak's position stays unaltered by variation in laser energy, while the peak's intensity may be impacted. The apparent existence of both PS and  $V_2O_5/Pd$  nanocrystal diffraction peaks in Fig. 2 indicates that  $V_2O_5/Pd$  nanostructure integrated into the porous structure of PS. At higher energy levels, the films also demonstrate a clear inclination towards a crystalline arrangement. The main determinant responsible for the morphological alteration observed is most likely the dynamic interplay of energy at the boundaries of the islands and the repulsive contact between these boundaries. The efficacy of pulsed laser deposition (PLD) as a deposition technique for producing vanadium pentoxide thin films on porous silicon has been successfully proven. Debye–Scherrer's formula is expressed as follows (Harb 2018).

$$D = \frac{0.89\lambda}{\beta \cos\theta} \quad (3)$$

where  $D$  represents the nanocrystallite size in nm, 0.89 is the Scherrer constant,  $\lambda$  is the X-ray wavelength in nm,  $\beta$  full width at half maximum and  $\theta$  is the Bragg angle. The crystallite size of  $V_2O_5/Pd$  NPs was calculated at the (200), (001), (101), and (111) peak

**Table 1** The X-ray diffraction measurements for  $V_2O_5/Pd$  thin film with different laser pulse energy

Laser energy (mJ/pulse)	Miller indices	$2\theta$ (deg.)	FWHM (rad)	crystallite size (nm)	$d_{hkl}$ (Å)
600	200	16.81	0.00621	22.173	1.054
	001	20.80	0.00907	15.520	0.853
	101	21.88	0.00765	20.166	0.811
	111	34.68	0.00692	21.043	0.516
	111	40.28	0.00901	16.095	0.447
800	200	16.6	0.00551	24.989	1.066
	001	20.8	0.00622	22.728	0.853
	101	23.28	0.00556	25.451	0.763
	111	34.4	0.00696	20.846	0.521
	111	40.4	0.00765	19.305	0.445
1000	200	16.64	0.00556	25.193	1.064
	001	20.72	0.00812	28.919	0.856
	101	21.84	0.00417	33.850	0.812
	111	33.88	0.00419	34.579	0.528
	111	40.56	0.00487	30.340	0.444

**Fig. 3** UV–Vis absorption spectra of  $V_2O_5/Pd$  obtained at different laser ablated energy via Nd: YAG laser at 1064 nm wavelength

intensity. The XRD patterns did not indicate any subordinate or contaminant phase development. Hence, it may be noticed that the porous structure did not influence the orthorhombic form of the wurtzite structure.

Table.1 show the laser intensity increases, a reduction in the full width at half maximum (FWHM) value has been observed, as well as an increase in the size of the crystalline structure.

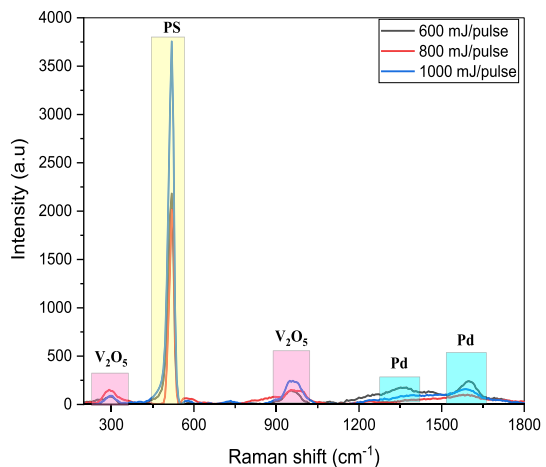
At room temperature, the optical absorption spectra were captured using a quartz plate with an optical path length of 6 mm. Figure 3 shows the absorbance spectra of  $V_2O_5/Pd$  samples created by PLD. A 1064 nm laser with energy of 600 mJ/pulse, 800 mJ/pulse,

and 1000 mJ/pulse was used in the PLD process. The absorption spectrum of vanadium pentoxide and palladium extends 220 nm to 340 nm, with films exhibiting strong peaks in the ultraviolet (UV) region. A parallel change in the peak's location towards a shorter wavelength happened as energy levels increased. It is also noted that the absorption peak at 1000 mJ/pulse has a higher level of sharpness. Regarding the different particle sizes within the examined range, the observed absorbance values showed a linear relationship. The ability to create particles of bigger size is enabled by the use of increased energy levels. The UV–Vis absorption spectra of composed  $V_2O_5$ :Pd NPs were investigated in the wavelength between (200–1100) nm. These NPs were synthesized using the PLD. UV–Vis spectra of  $V_2O_5$ :Pd NPs, which were synthesized through PLD at 300 pulses with varying laser energy (600, 800, 1000) mJ/pulse. The spectra show strong absorption between (220–340 nm) and shifts towards shorter wavelengths (blue shift) with increasing the laser energy due to reducing the size of the nanoparticles. A significant decrease in the absorption below 360nm is observed and the absorption edge is shifted toward longer wavelengths with increasing the laser energy. Moreover, the intensity of absorption peaks is increased with laser energy due to the high concentration of nanoparticles. This can be explained as; by delivering more energy to the target leads to produce intense plasma plume and ablating larger amount of material so that the nanoparticles become denser on substrate.

Figure 4 shows the Raman spectra of  $V_2O_5$ /Pd thin films deposited onto porous silicon substrates using PLD. The spectra were gathered from  $200\text{ cm}^{-1}$  to  $1800\text{ cm}^{-1}$ , covering the entire spectrum.

Five characteristic peaks are seen at  $292\text{ cm}^{-1}$ ,  $519\text{ cm}^{-1}$ ,  $953\text{ cm}^{-1}$ ,  $1362\text{ cm}^{-1}$  and  $1588\text{ cm}^{-1}$ . The main peak at  $519\text{ cm}^{-1}$  is associated to the PS phonon mode (Richter et al. 1981). The peak observed at a frequency of  $992\text{ cm}^{-1}$  can be attributed to the stretching mode of terminal oxygen ( $V=O$ ), which arises from unshared oxygen atoms. The observed peak at  $292\text{ cm}^{-1}$  can be ascribed to the bending vibration of the ( $V=O$ ) bonds. Furthermore, the lack of a discernible peak at  $850\text{ cm}^{-1}$  suggests that the films under investigation are not hydrated ( $V_2O_5 \cdot H_2O$ ), as the presence of such hydration would generally manifest as an impurity (Lee et al. 2016; Harb and Mutlak 2022b; Sanchez et al. 1982). The two peaks observed at  $1362$  and  $1588\text{ cm}^{-1}$  are attributed to the presence of Pd (Fast sensing of imidacloprid residue in tea using surface-enhanced Raman scattering by comparative multivariate calibration. 2019). The spectral peaks have identical frequencies. The bands'

**Fig. 4** Raman spectra of the  $V_2O_5$ /Pd grown on PS substrate, with different laser ablated energy via Nd: YAG laser at 1064 nm wavelength

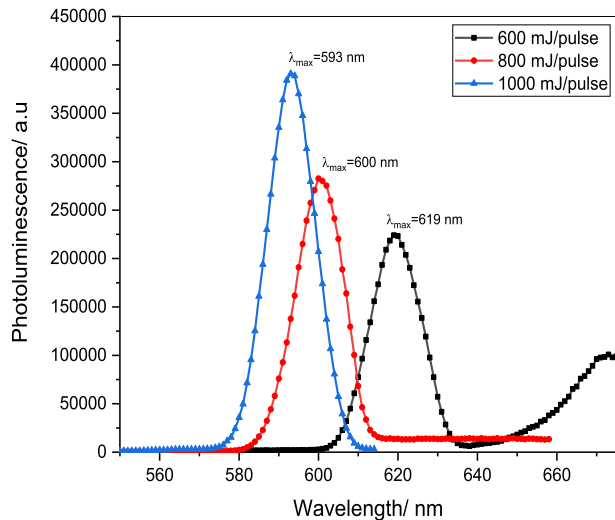




intensity undergoes shifts due to variation in the energy of the laser pulse, as stated by the referenced source (Ahmed et al. 2021). The augmentation in the energy of the laser pulse resulted in alterations in the spectral properties of the films, subsequently producing enhancements in the resolution and efficacy of the Raman bands. The observed evolutionary process leads to peak band alterations, leading to enhanced efficacy and specificity. The presence of well-defined peaks can be used as evidence to suggest an augmentation in the level of crystallinity. The bands have exhibited enhanced strength and have achieved a greater level of differentiation. The identification of crystalline forms can be inferred from the dataset by examining prominent peaks.

Photoluminescence spectroscopy was employed to investigate the optical characteristics of  $V_2O_5/Pd$  thin films fabricated using PLD at a wavelength of 1064 nm on PS substrate. In Fig. 5, the alterations in the intensity of photoluminescence (PL) are depicted in relation to frequency across different instances. The identification of the peaks corresponding to the PL wavelengths of 619 nm, 600 nm, and 593 nm was achieved with ease. Subsequently, the energy gap values were determined as 2.00, 2.06, and 2.09 eV, respectively. This analysis was conducted by employing laser pulse energies of 600 mJ/pulse, 800 mJ/pulse, and 1000 mJ/pulse. The crystallized  $V_2O_5/Pd$  composite has comparatively elevated energy gap of 2.09 eV. The emission detected at a wavelength of 590 nm could potentially arise from a transition between the conduction and valence bands. A comparison of the photoluminescence emission spectra of  $V_2O_5/Pd$  thin films deposited on porous silicon at room temperature with different laser energies at an excitation wavelength of 400 nm are presented in Fig. 5. The  $V_2O_5/Pd$  exhibits an extreme PL emission band broadening centered at a visible wavelength of 619 nm, 600 nm, and 593, which reveals the excellent quality of the  $V_2O_5/Pd$  structure. This blue shift in  $V_2O_5/Pd/PS$  structure is the consequence of the radiative recombination of electron–hole pairs induced by photoexcitation and confined within Si nanocrystals. The quantum size effect changes the electronic spectrum due to this confinement. Moreover, we notice an increase in the emission of the intense  $V_2O_5/Pd/PS$  peak attributable to the surface oxidization caused by the  $V_2O_5$  layer. However, the red emission regions of the  $V_2O_5/Pd$  layer/PS exhibit a blue shift with increasing laser energy of the PLD technique. It may be due to nanostructure size and enhanced at the

**Fig. 5** PL spectra for  $V_2O_5/Pd$  thin films formed by PLD at 1064 nm with varied laser ablated energy



$V_2O_5$  layer interface between the Pd layer and the porous silicon substrate. Clearly, the PL spectra excitation value of 400 nm with a blue shift in PL spectra is the consequence of the radiative recombination of electron–hole pairs induced by photoexcitation and confined within Si nanocrystals. On the other hand, the line form of the PL spectra may be used to precisely identify the electronic state distribution and electronic structure. With increasing laser pulse energy 600 mJ/pulse to 1000 mJ/pulse, is obvious that the PL peak has shifted slightly blue, resulting in a little increase in the energy band gap ( $E_g$ ) (2.00, 2.06, and 2.09) eV. The Moss–Burstein effect (Suresh 2016) describes how the value of the energy gap grows as laser energy increases owing to an increase in Fermi level (EF). For optoelectronic applications, the move to shorter wavelengths is beneficial. Tables 2 and 3 display the gas sensor characteristics in  $H_2S$  and  $NO_2$  gases of  $V_2O_5/Pd$ , respectively.

The surface morphology of thin films composed of porous silicon and  $V_2O_5/Pd$  was investigated using Field Emission-Scanning Electron Microscopy (FE-SEM). The films were fabricated by the technique of Pulsed Laser Deposition PLD, employing varying laser energy. Field Emission Scanning Electron Microscopy is renowned for its high capacity to produce precise and clearly defined pictures at exceedingly high levels of magnification. Consequently, FE-SEM is considered a viable technique for estimating the average grain size of these particular surfaces. The given specimen exhibits a porous morphology that is distinguished by the presence of spherical particles composed of powder. When exposed to 600 mJ/pulse of energy, the surface grains exhibited an average size of approximately 200 nm. This size increased to around 250 nm when the energy exposure was increased to 800 mJ/pulse, and further increased to approximately 300 nm when the energy exposure was raised to 1000 mJ/pulse. The aforementioned observation indicates the existence of a discernible surface grain attribute, as depicted in Fig. 6. The enhancement in the homogeneity of particle size and energy pulse resulted in a corresponding augmentation in the dimensions of surface grains. This facilitated the amalgamation of adjacent tiny crystals, leading to the formation of larger surface grains. This suggests that the particular configuration of

**Table 2** The gas sensor characteristics result to  $H_2S$  gas of  $V_2O_5/Pd$  prepared using PLD with different laser ablated energy

Laser energy (mJ/pulse)	T (°C)	Sensitivity (%)	Response time (sec)	Recover time (sec)
600	30	4.271	29.07	103.95
	100	7.038	14.76	74.25
	150	27.312	28.98	54.45
	200	21.651	15.3	40.50
	250	16.279	19.71	67.50
800	30	19.259	20.61	56.25
	100	96.969	22.05	70.20
	150	29.613	21.15	41.85
	200	15.521	16.29	42.75
	250	11.578	19.35	47.25
1000	30	31.818	26.11	90.90
	100	34.693	27.63	66.60
	150	60.012	22.41	63.90
	200	28.378	23.04	68.85
	250	22.962	32.04	55.35

**Table 3** The gas sensor characteristics result to NO<sub>2</sub> gas of V<sub>2</sub>O<sub>5</sub>/Pd prepared using PLD with different laser ablated energy

Laser energy (mJ/pulse)	T (°C)	Sensitivity (%)	Response time (sec)	Recover time (sec)
600	30	9.090	28.98	153.0
	100	17.187	17.73	97.20
	150	18.247	26.19	161.10
	200	17.307	19.98	189.00
	250	14.838	17.19	48.60
800	30	23.694	21.33	153.00
	100	32.885	29.16	187.20
	150	34.174	24.03	180.00
	200	22.330	18.02	61.20
	250	15.662	17.10	52.20
1000	30	14.285	28.80	167.00
	100	40.012	27.81	101.70
	150	31.818	22.23	85.50
	200	18.674	19.08	78.30
	250	15.492	19.26	45.00

the film is anticipated to optimize the adsorption process of H<sub>2</sub>S and NO<sub>2</sub> molecules. The observed affinity for H<sub>2</sub>S and NO<sub>2</sub> molecule adsorption can be attributed to the structural properties of the film, which is characterized by a high density of tiny pores and a large surface area. This suggests that the aforementioned film demonstrates a positive inclination towards gases.

The weight percentages of vanadium (V), oxygen (O), and palladium (Pd) in the acquired samples were analyzed at various laser energy levels and laser wavelengths of 1064 nm, as illustrated in Fig. 6. The measured percentages for vanadium (V), oxygen (O), and palladium (Pd) were found to be (21.35, 26.24, 30.56) wt% V, (27.41, 28.46, 20.32) wt% O, and (7.56, 8.35, 10.91) wt% Pd, respectively. The provided findings are consistent with the expected stoichiometry seen in the synthesized V<sub>2</sub>O<sub>5</sub>/Pd on PS substrate samples. There were no further peaks observed that may be attributed to contaminants, suggesting that the V<sub>2</sub>O<sub>5</sub>/Pd thin layer produced in this investigation is of high quality.

### 3.2 Gas-sensing properties

The objective of this research is to examine the sensitivity fluctuations of a gas sensor that employs a precipitated V<sub>2</sub>O<sub>5</sub>/Pd PS material when subjected to H<sub>2</sub>S and NO<sub>2</sub> gases. The investigation will focus on analyzing the sensitivity variation of the sensor at its operational temperature. This analysis will involve subjecting the sensor to three distinct pulse laser deposition energies: 600 mJ/pulse, 800 mJ/pulse, and 1000 mJ/pulse. Figure 7, present graphical representations of the sensitivity of the gas sensor measurement, as well as the rate of response and recovery time, across a wide range of operating temperatures, specifically ranging from 30 to 250 °C.

The utilization of mathematical formulae was helpful in determining the characteristics of these curves (Harb and Mutlak 2023).

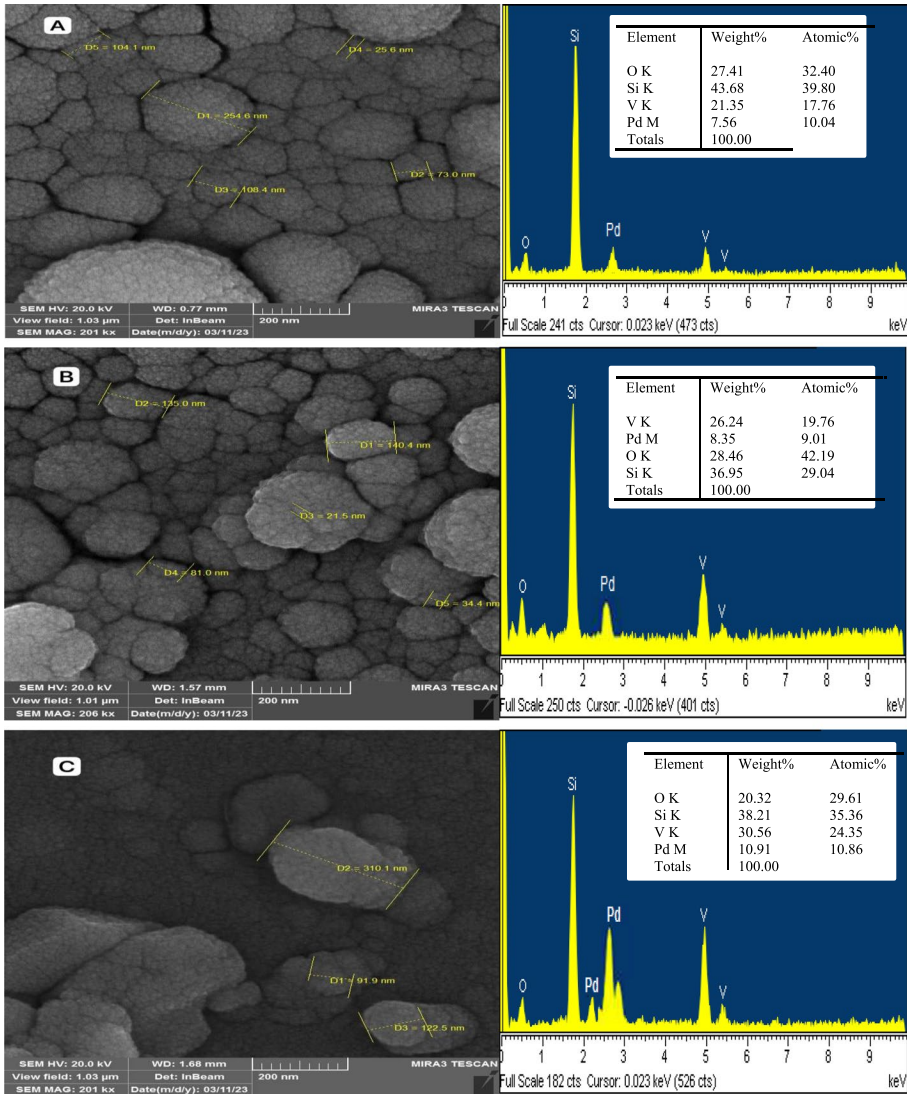


**Fig. 6** FE-SEM images related to the samples  $V_2O_5/Pd$  NPs on PS with laser ablated energy **A** 600 mJ/pulse, **B** 800 mJ/pulse **C** 1000 mJ/pulse

$$S = \frac{R(\text{on}) - R(\text{off})}{R(\text{on})} \times 100\% \tag{4}$$

$$\text{Response time} = |t_{\text{gas}}(\text{on}) - t_{\text{gas}}(\text{off})| * 0.9 \tag{5}$$

$$\text{Recover time} = |t_{\text{gas}}(\text{off}) - t_{\text{gas}}(\text{on})| * 0.9 \tag{6}$$

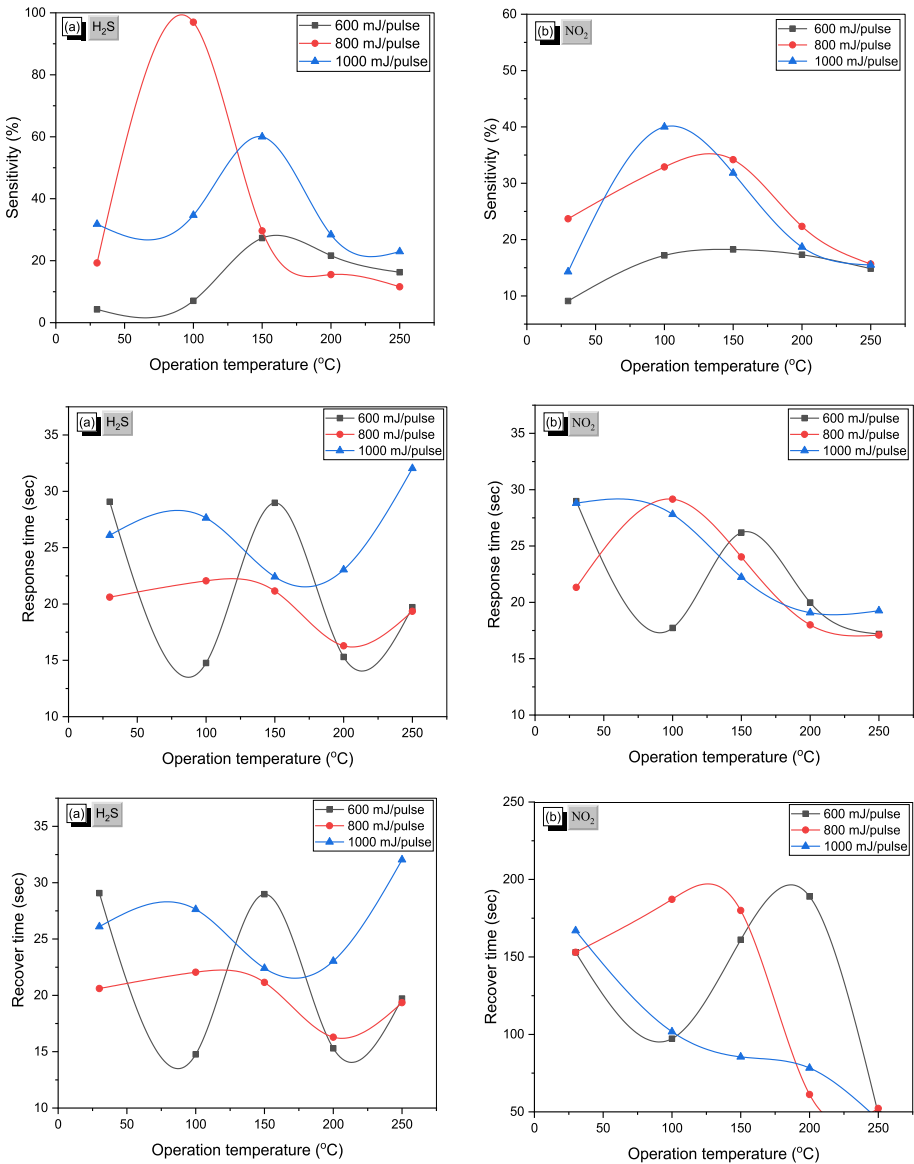


**Fig. 7** The sensitivity, response time and recover time of **a** H<sub>2</sub>S and **b** NO<sub>2</sub> gases of V<sub>2</sub>O<sub>5</sub>/Pd NPs prepared using PLD with different laser ablated energy via Nd: YAG laser at 1064 nm wavelength

The study focuses on several factors, including sensitivity (S), pre-exposure resistance to H<sub>2</sub>S and NO<sub>2</sub> gases (R on), and post-exposure resistance to these gases (R off).

This study provides evidence that sensors composed of V<sub>2</sub>O<sub>5</sub>/Pd display reversible alterations in electrical resistance upon the activation and deactivation of H<sub>2</sub>S and NO<sub>2</sub> gas flow. The resistance values of the sensors exhibit a reduction in the presence of air as the operational temperature rises, a characteristic commonly found in ceramic materials.

Following the introduction of gas into the test chamber, the resistance of the sensor exhibited an increase, ultimately reaching a condition of saturation. Following the discontinuation of the gas flow, a significant decrease in the resistance reported by the sensor was observed. The temperature dependence is attributed to two primary factors. One aspect to consider is that the processes of adsorption, desorption, and diffusion between the semi-conducting oxide surface and the target gas are all thermally stimulated reactions. Therefore, the reaction rate exhibits a positive correlation with the rise in temperature during the course of the experiment. In contrast, it is observed that electrons in oxide semiconductors have a higher probability of acquiring the necessary energy to transition from the valence band to the conduction band when exposed to higher temperatures. Consequently, there is a rise in the abundance of unbound electrons, resulting in a commensurate decrease in electrical resistance. The ideal temperature, at which the electrical resistance (and thus the sensing response), is highest, is achieved through a combination of the thermally activated process and the heightened likelihood of free-electron production with increasing temperature (Kim and Lee 2014; Ahlers et al. 2005).

Figure 7 illustrates the sensitivity of  $V_2O_5/Pd$  sensors towards  $H_2S$  and  $NO_2$  gases throughout a temperature span ranging from 30 to 250 degrees Celsius. The presented image illustrates the ability to detect Hydrogen Sulfide ( $H_2S$ ) and Nitrogen Dioxide ( $NO_2$ ) gases in the atmosphere under low-temperature conditions. The accompanying table and graph provide evidence of a significant sensitivity to both gases, even at room temperature. Specifically, at a temperature of 30°C and an energy level of 1000 mJ, the detection sensitivity for  $H_2S$  was found to be 31%, while for  $NO_2$ , it was 23.69% at 800 mJ. Nevertheless, the maximum value was seen at temperatures of 150°C and 100°C. It was clear that increasing  $H_2S$  gas sensitivity with increasing temperature up to 100°C and after decreasing when increasing temperature, the increase in sensitivity as temperature rises could be due to grain growth of  $V_2O_5/Pd$  nanoparticle, which leads to a decrease in open porosity. The maximum sensitivity 96.96 in laser pulse energy 800 mJ to concentration is 50 ppm but  $NO_2$  test gas sensitivity 40% at 100 °C of energy 1000 mJ to concentration is 62 ppm.

The  $V_2O_5/Pd$  sensors have a time-dependent response and demonstrate a high sensitivity towards detecting  $H_2S$  and  $NO_2$  concentrations in the surrounding atmosphere. Following the successful stabilization of the initial resistance, the introduction of gases into the enclosed chamber of the batch system occurred, and subsequent expulsion of the gas was carried out after a sustained duration of five minutes. At 1000 mJ/pulse and 250 °C, the  $H_2S$  gas sensor has a maximum reaction time of 32.04 s and a minimum recover time of 40.5 s at 600 mJ and 200 °C. The gas sensor's maximum reaction time for  $NO_2$  is 29.16 s at a temperature of 100 °C and an energy level of 800 mJ/pulse. Similarly, at a temperature of 250 °C and an energy level of 1000 mJ/pulse, the sensor exhibits a minimum recovery time of 45 s. The increased sensitivity can be elucidated by employing Field Emission Scanning Electron Microscopy (FESEM) images for thin films consisting of ( $V_2O_5/Pd$ ). The increased intensity of laser energy pulses can induce a higher quantity of grain boundaries, which are regions susceptible to gas sensitivity. As a result, an increased level of sensitivity may occur due to the impact of grain size. The microstructure and surface area are considered to be the key elements that influence the characteristics of the sensor. The presence of a porous structure facilitates an increased surface area, thereby providing a greater number of reactive sites for electrons, oxygen, and gases. Furthermore, the presence of a network of linked gaps and pores among the offers several pathways for gas diffusion and electron transport, which is in contrast to the limited channels available in a dense film. Hence, the utilization of  $V_2O_5/Pd$  exhibiting substantial porosity and a significant surface area is imperative in order to augment the sensitivity of gas sensors. The gas sensing

characteristics of  $V_2O_5$  are significantly influenced by the porous structure within and the interface area (Bai et al. 2013).

Films that possess a porous structure have a notable abundance of atoms located at the boundaries and interfaces within the pores. This observation suggests that the microstructure of these films is highly suitable for gas-sensing applications. The increased sensitivity of a mesoporous sensor can be explained by the fact that all of the surface adsorption sites are exposed to the surrounding chemicals. Both adsorption and desorption are thermal processes that are subject to temperature influences. The efficacy of the  $V_2O_5/Pd$  NPs sensor's recovery is maximized at lower temperatures, while its performance exhibits a progressive decline with increasing temperatures. In general, increased operating temperature led to lower response and recovery times. As the operating temperature rises, electron transfer between the conductor band and the surface Fermi level accelerates, aiding the adsorption process and, as a consequence, shortening the recovery time. In general, increased operating temperature led to lower response and recovery times. As the operating temperature rises, electron transfer between the conductor band and the surface Fermi level accelerates, aiding the adsorption process and, as a consequence, shortening the recovery time. The utilization of  $V_2O_5/Pd$  thin films holds great potential for the development of superior miniaturized chemical sensors. Moreover, present studies show that the PLD and parameters of synthesizing have an important effect on the performance of gas sensor devices, especially with increased laser-ablated energy. Hence, the optimization of the gas sensor, as well as good control of environmental factors (i.e., temperature) is extremely important for the sensitivity efficiency and performance of  $H_2S$  and  $NO_2$  may vary the gas sensor properties devices. Finally, even though gas sensor devices are still far from reaching the market and need advanced technical development, the combination of these systems with new microfabricated gas sensors showcase great potential for the practical and low-cost in future industry applications.

## 4 Conclusions

In summary, the findings of this study demonstrate that gas sensors using a porous silicon layer combined with a  $V_2O_5/Pd$  composite have enhanced sensitivity and selectivity towards  $H_2S$  and  $NO_2$  gases when fabricated using the pulsed laser deposition (PLD) process. The study investigated the effects of laser-ablated energy on elemental composition. The findings suggest that the modulation of laser settings has the potential to exert control over the thickness and shape of the film. The  $V_2O_5/Pd$  prepared samples morphology and average grain size depended on the laser energy used during deposition. The distinction grain size measurements, was predicted because FE-SEM shows the grains without considering the presence of structural defects. In contrast, determines the extent of the defect-free quantity at high laser energy. The study investigated the influence of laser-ablated energy on elemental composition. The utilization of ideal laser pulse energy promotes the fusion of neighboring tiny crystals, resulting in the formation of significantly larger surface grains. The sensitive nature of the  $V_2O_5/Pd$  thin layer was shown to increase as the pulse laser intensity was increased during the deposition process. The impact of Pd on the kinetics of  $V_2O_5$  nanoparticles' growth was investigated, revealing that Pd has the ability to enhance sensitivity while concurrently reducing the operational temperature. In addition, the nanoparticles demonstrated significant sensitivity even at room temperature conditions. The sensor exhibits a highly favorable reaction to gases within its detectable range,

achieving a response rate of 96% and demonstrating rapid response and recovery times of just a few seconds. The sensor exhibits enhanced sensitivity, rapid response, high stability, high selectivity, low temperature operability, and superior performance in comparison to the sensors documented in existing literature. Consequently, these films exhibit considerable potential as a straightforward, resilient, and economical approach for detecting H<sub>2</sub>S and NO<sub>2</sub> gases at low concentrations.

**Acknowledgements** The authors would like to thank University of Baghdad -Iraq for the logistic supports this work.

**Author contributions** M.A and F.M. conceived of the presented idea. F.M. supervised the findings of this work. M.A discussed the results. All authors conducted the experiments. M.A and F.M provided critical feedback and helped shape the research, analysis, and manuscript.

**Funding** Not applicable.

**Data availability** The data used to support the findings of this study are included within the article.

## Declarations

**Conflict of interest** The authors have declared no conflict of interest.

**Ethics approval and consent to participate** Not applicable.

**Consent for publication** Not applicable.

## References

- A. Bouzidi, N.; Benramdane, A.; Nakrela, C.; Mathieu, B.; Khelifa, R.; Desfeux, A.; DaCosta, First synthesis of vanadium oxide thin films by spray pyrolysis technique, *Adv. Mater. Res.* (2002) 141–147.
- Aawani, E., Memarian, N., Dizaji, H.R.: Synthesis and characterization of reduced graphene oxide– V<sub>2</sub>O<sub>5</sub> nanocomposite for enhanced photocatalytic activity under different types of irradiation. *J. Phys. Chem. Solids* **125**, 8–15 (2019)
- Abd-Alghafour, N.M., Ahmed, N.M., Hassan, Z., Almessiere, M.A., Bououdina, M., Al-Hardan, N.H.: High sensitivity extended gate effect transistor based on V<sub>2</sub>O<sub>5</sub> nanorods. *J. Mater. Sci. Mater. Electron.* **28**, 1364–1369 (2017)
- Abed, M.A., Mutlak, F.A.-H., Ahmed, A.F., Nayef, U.M., Abdulridha, S.K., Jabir, M.S.: Synthesis of Ag/Au core/shell nanoparticles by laser ablation in liquid and study of their toxicity on blood human components. *J. Phys. Conf. Ser.* **1795**, 012013 (2021)
- Abood, H.K., Mutlak, F.A.-H.: Structural, morphological and optical properties of n-type porous silicon-effect of etching current density. *IOP Conf. Ser. Mater. Sci. Eng.* **757**, 012065 (2020)
- Ahlers, S., Muller, G., Doll, T.: A rate equation approach to the gas sensitivity of thin film metal oxide materials. *Sens. Actuators B* **107**, 587–599 (2005)
- Ahmed, A., Aadim, K., Yousef, A.: Spectroscopic study of AL nitrogen plasma produced by DC glow discharge. *Iraqi J. Sci.* **59**, 494 (2018)
- Ahmed, A.F., Abdulameer, M.R., Kadhim, M.M., Mutlak, F.A.-H.: Plasma parameters of Au nano-particles ablated on porous silicon produced via Nd-YAG laser at 355 nm for sensing NH<sub>3</sub> gas. *Optik* **249**, 168260 (2022)
- Ahmed, A., Yaseen, W., Abbas, Q., Mutlak, F.: Plasma treatment effect on SnO<sub>2</sub>–GO nano-heterojunction: fabrication, characterization and optoelectronic applications. *Appl. Phys. A* **127**, 746 (2021)
- Alam, M.M., Uddin, M.T., Asiri, A.M., Rahman, M.M., Islam, M.A.: Development of reproducible thiourea sensor with binary SnO<sub>2</sub> / V<sub>2</sub>O<sub>5</sub> nanomaterials by electrochemical method. *Arab. J. Chem.* **13**, 5406–5416 (2020)
- Alber, A., Mutlak, F.: The role of various etching time in Si nanostructures for ultra-high sensitivity photo-detector. *Optik* **265**, 169427 (2022)



- Alber, A.S., Mutlak, F.A.H.: A novel laser-assisted approach for synthesis of AuNPs/PS nanostructures as photodetector". *J. Opt.* **52**, 1477 (2023). <https://doi.org/10.1007/s12596-022-00958-1>
- Amiri, V., Roshan, H., Mirzaei, A., Neri, G., Ayes, A.I.: Nanostructured metal oxide-based acetone gas sensors: a review. *Sensors* **20**, 3096 (2020)
- Aswad, M.A., Mutlak, F.A.H., Jabir, M.S., Abdulridha, S.K., Ahmed, A.F., Nayef, U.M.: Laser assisted hydrothermal synthesis of magnetic ferrite nanoparticles for biomedical applications. *J. Phys. Conf. Ser.* **1795**, 012030 (2021)
- Bai, S., Sun, C., Guo, T., Luo, R., Lin, Y., Che, A., Sun, L., Zhang, J.: Low temperature electrochemical deposition of nanoporous ZnO thin films as novel NO<sub>2</sub> sensors. *Electrochim. Acta* **90**, 530–534 (2013)
- Eric, K., Dimitris, E., Gin, J.: Phase changeable vanadium dioxide (VO<sub>2</sub>) thin films grown from vanadium pentoxide (V<sub>2</sub>O<sub>5</sub>) using femtosecond pulsed laser deposition. *AIP Adv.* **10**, 065225 (2020)
- Fardindoost, S.; Irajizad, A.; Rahimi, F.; Ghasempour, R.: Pd doped WO<sub>3</sub> films prepared by sol-gel process for hydrogen sensing. *Int. J. Hydrogen Energy* 2010. <http>
- Gross, P.-A., Jaramillo, T., Pruitt, B.: Cyclic-voltammetry-based solid-state gas sensor for methane and other VOC detection. *Anal. Chem.* **90**, 6102–6108 (2018)
- Harb, N.: The structure and optical properties of Ag doped CdO thin film prepared by pulse laser deposition (PLD). *Baghdad Sci. J.* **15**, 3 (2018)
- Harb, N., Mutlak, F.A.-H.: Production and characterization of porous silicon via laser-assisted etching: effect of gamma irradiation. *Optik* **246**, 167800 (2021)
- Harb, N.H., Mutlak, F.A.-H.: Synthesis and characterization of vanadium pentoxide nanospheres by pulsed laser deposition: effect of laser ablated energy on photodetectors properties. *Optik* **257**, 168842 (2022)
- Harb, N.H., Mutlak, F.A.-H.: Effect of laser wavelength on the characterization of V<sub>2</sub>O<sub>5</sub> NPs/PS photodetector synthesized by pulsed laser deposition. *Optik* **258**, 168953 (2022)
- Harb, N.H., Mutlak, F.A.H.: Gas sensing characteristics of WO<sub>3</sub>NPs sensors fabricated by pulsed laser deposition on PS n-type. *J. Opt.* **52**(1), 323–331 (2023)
- Hou, T.-F., Johar, M.A., Boppella, R., Hassan, M.A., Patil, S.J., Ryu, S.-W., Lee, D.-W.: Vertically aligned one-dimensional ZnO/V<sub>2</sub>O<sub>5</sub> core-shell hetero-nanostructure for photoelectrochemical water splitting. *J. Energy Chem.* **49**, 262–274 (2020)
- Huotari, J., Lappalainen, J., Puustinen, J., Lloyd Spetz, A.: Gas sensing properties of pulsed laser deposited vanadium oxide thin films with various crystal structures". *Sens. Actuators B: Chem.* **187**, 386–394 (2013)
- J. Huotari, A.; Lloyd Spetz, J.; Lappalainen, "Gas sensing properties of pulsed laser deposited vanadium oxide thin films", IMCS 2012 – The 14th International Meeting on Chemical Sensors.
- Jolly Bose, R.; Ilyaskutty, N.; Tan, K.S.; Rawat, R.S.; Matham, M.V.; Kohler, H., Mahadevan Pillai, V.P. Hydrogen sensors based on Pt-loaded WO<sub>3</sub> sensing layers. *EPL* 2016.
- Julien, C., Haro-Poniatowski, E., Camacho-López, M.A., Escobar-Alarcón, L., Jiménez-Jarquín, J.: Growth of V<sub>2</sub>O<sub>5</sub> thin films by pulsed laser deposition and their applications in lithium microbatteries. *Mater. Sci. Eng.: B* **65**, 170–176 (1999)
- Jwar, A.J., Nayef, U.M., Mutlak, F.A.H.: Study effect of magnetic field on Au-TiO<sub>2</sub> core-shell nanoparticles via laser ablation deposited on porous silicon for photodetector. *Plasmonics* **18**, 595–605 (2023)
- Jwied, D., Mutlak, F.A.-H., Nayef, U.: Improvement of responsivity of C: Se nanoparticles ablated on porous silicon. *Optik* **241**, 167222 (2021)
- Jwied, D.H., Nayef, U.M., Mutlak, F.A.-H.: Synthesis of C: Se nanoparticles ablated on porous silicon for sensing NO<sub>2</sub> and NH<sub>3</sub> gases. *Optik* **241**, 167013 (2021)
- Jwied, D.H., Nayef, U.M., Mutlak, F.A.H.: Synthesis of C: Se nanoparticles via laser ablated with magnetic field on porous silicon for gas sensor applications. *Optik* **242**, 167207 (2021)
- Kei, I., Toshio, O., Makoto, M., Nobuyuki, M., Sh Hiromichi Akio, N.: EXAFS analysis of vanadium oxide thin over layers on silica prepared by chemical vapor deposition. *J. Chem. Soc.* **88**(4), 625–630 (1992)
- Kh Hammad, Q., Ayyash, A.N., Mutlak, F.A.-H.: Improving SERS substrates with Au/Ag-coated Si nanostructures generated by laser ablation synthesis in PVA. *J. Opt.* **52**, 1528 (2023). <https://doi.org/10.1007/s12596-022-00971-4>
- Khudiar, S.S., Nayef, U.M., Mutlak, F.A.-H.: Preparation and characterization of ZnO nanoparticles via laser ablation for sensing NO<sub>2</sub> gas. *Optik* **246**, 167762 (2021)
- Kim, H.-J., Lee, J.-H.: Highly sensitive and selective gas sensors using p-type oxide semiconductors: overview. *Sens. Actuators B* **192**, 607–627 (2014)
- Laubach, S., Schmidt, P.C., Thißen, A., Fernandez-Madrugal, F.J., Wu, Q.-H., Jaegermann, W., Klemm, M., Horn, S.: Theoretical and experimental determination of the electronic structure of V<sub>2</sub>O<sub>5</sub>, reduced V<sub>2</sub>O<sub>5-x</sub> and sodium intercalated NaV<sub>2</sub>O<sub>5</sub>. *Phys. Chem. Chem. Phys.* **9**, 2564–2576 (2007)
- Le, T.K., Kang, M., Kim, S.W.: A review on the optical characterization of V<sub>2</sub>O<sub>5</sub> micro-nanostructures. *Ceram. Int.* **45**, 15781–15798 (2019)

- Lee, S., Ivanov, I.N., Keum, J.K., Lee, H.N.: Epitaxial stabilization and phase instability of VO<sub>2</sub> polymorphs. *Sci. Rep.* **6**, 19621 (2016)
- Lu, Z., Levi, M.D., Salitra, G., Gofer, Y., Levi, E., Aurbach, D.: Basic electroanalytical characterization of lithium insertion into thin, well-crystallized V<sub>2</sub>O<sub>5</sub> films. *J. Electroanal. Chem.* **491**(1), 211–221 (2000)
- Mane, A.A., Maldar, P.S., Dabhole, S.H., Nikam, S.A., Moholkar, A.V.: Effect of substrate temperature on physicochemical and gas sensing properties of sprayed orthorhombic V<sub>2</sub>O<sub>5</sub> thin films. *Measurement* **131**, 223–234 (2019)
- Matthe, R., Muhammad, K.H., Zubair Khan, M., Hammad, R., Humira, R.: V<sub>2</sub>O<sub>5</sub> thin films deposited by sol-gel and indigenously developed spin coating system. *Arab. J. Sci. Eng.* **43**, 407–413 (2018)
- Mirzaei, A., Janghorban, K., Hashemi, B., Bonyani, M., Leonardi, S.G., Neri, G.: A novel gas sensor based on ag/fe<sub>2</sub>o<sub>3</sub> core-shell nanocomposites. *Ceram. Int.* **42**, 18974–18982 (2016)
- Mounasamy, V., Mani, G.K., Madanagurusamy, S.: Vanadium oxide nanostructures for chemiresistive gas and vapour sensing: a review on state of the art. *Microchim. Acta* **187**, 1–29 (2020)
- Mutlak, F.A.-H.: Photovoltaic enhancement of Si micro-and nanostructure solar cells via ultrafast laser texturing. *Turkish J. Phys.* **38**, 130–135 (2014)
- Mutlak, F.A.H., Jaber, M., Emad, H.: Effect of laser pulse energy on the characteristics of Au nanoparticles and applications in medicine. *Iraqi J. Sci.* **58**, 2364–2369 (2017)
- Mutlak, F.A.-H., Jamal, R.K., Ahmed, A.F.: Pulsed laser deposition of TiO<sub>2</sub> nanostructures to verify the linear and non-linear optical characteristics. *Iraqi J. Sci.* **62**(2), 517–525 (2021)
- Mutlak, F.A.H., Taha, A.B., Nayef, U.M.: Synthesis and characterization of SnO<sub>2</sub> on porous silicon for photoconversion. *Silicon* **10**(3), 967–974 (2017)
- Naseri, N.; Kim, H., Choi, W., Moshfegh, A.Z. Implementation of Ag nanoparticle incorporated WO<sub>3</sub> thin film photoanode for hydrogen production. *Int J Hydrogen Energy* 2013.
- Ozdemir, S., Gole, J.L.: The potential of porous silicon gas sensors. *Curr. Opin Solid State Mater. Sci. Semicond. Process.* **11**, 92–100 (2007)
- Quansheng Chen, Md., Hassan, M., Jing, Xu., Zareef, M., Li, H., Yi, Xu., Wang, P., Agyekum, A.A., Kut-sanedzie, F.Y.H., Viswadevarayalu, A.: Fast sensing of imidacloprid residue in tea using surface-enhanced Raman scattering by comparative multivariate calibration. *Spectrochim Acta Part A Mol. Biomol. Spectrosc.* **211**, 86–93 (2019)
- Rajesh, K., Santhanalakshmi, J.: Design and development of graphene intercalated V<sub>2</sub>O<sub>5</sub> nanosheets based electrochemical sensors for effective determination of potentially hazardous 3,5-dichlorophenol. *Mater. Chem. Phys.* **199**, 497–507 (2017)
- Rashid, T.M., Nayef, U.M., Jabir, M.S., Mutlak, F.A.: Study of optical and morphological properties for Au-ZnO nanocomposite prepared by Laser ablation in liquid. *J. Phys. Conference Series* **1795**, 012041 (2021)
- Rashid, T.M., Nayef, U.M., Jabir, M.S., Mutlak, F.A.H.: Synthesis and characterization of Au:ZnO (core:shell) nanoparticles via laser ablation. *Optik* **244**, 167569 (2021)
- Rathika, R.; Kovendhan, M.; Joseph, D.P.; Pachaiappan, R.; Kumar, A.S.; Vijayarangamuthu, K.; Venkateswaran, C.; Asokan, K.; Jeyakumar, S.J. Tailoring the properties of spray deposited V<sub>2</sub>O<sub>5</sub> thin films using swift heavy ion beam irradiation. *Nucl. Eng. Technol.* 2020.
- Richter, H., Wang, Z., Ley, L.: The one phonon Raman spectrum in microcrystalline silicon. *Solid State Commun.* **39**(5), 625–629 (1981)
- Sanchez, C., Livage, J., Lucazeau, G.: Infrared and Raman study of amorphous V<sub>2</sub>O<sub>5</sub>. *J. Raman Spectrosc.* **1**, 12 (1982)
- Shaikshavali, P., Ch Rodney, Z., Yang, E., Eldho, S.M.: Amorphous vanadium oxide thin films as stable performing cathodes of lithium and sodium-ion batteries. *Nanoscale Res. Lett.* **13**, 363 (2019)
- Shobha, N.; Birajdar,.; Parag V. Adhyapak.; 'Palladium-decorated vanadium pentoxide as NO<sub>x</sub> gas sensor', *Ceramics Int.* 2020, 46(17).
- Singh, N., Umar, A., Singh, N., Fouad, H., Alotman, O.Y., Haque, F.Z.: Highly sensitive optical ammonia gas sensor based on Sn doped V<sub>2</sub>O<sub>5</sub> nanoparticles. *Mater. Res. Bull.* **108**, 266–274 (2018)
- Slewa, L.H., Abbas, T.A., Ahmed, N.M.: Effect of Sn doping and annealing on the morphology, structural, optical, and electrical properties of 3d (micro/nano) V<sub>2</sub>O<sub>5</sub> sphere for high sensitivity ph-egfet sensor. *Sens. Actuators B Chem.* **305**, 127515 (2020)
- Suresh, R.: Effect of post-growth annealing on the structural optical and electrical properties of V<sub>2</sub>O<sub>5</sub> nanorods and its fabrication, characterization of V<sub>2</sub>O<sub>5</sub>/p-Si junction diode. *Mater. Sci. Semicond. Process.* **41**, 497–507 (2016)
- West, K., Zachau-Christiansen, B., Skaarup, S.V., Poulsen, F.W.: Lithium insertion in sputtered vanadium oxide film. *Solid State Ion.* **57**(1), 41–47 (1992)
- Yousef, A., Ahmed, A.: Spectroscopic analysis of DC-nitrogen plasma produced using copper electrodes. *Iraqi J. Sci.* **62**, 3560 (2021)

Yıldırım, M.A., Tuna Yıldırım, S., Çağırtekin, A.O., Karademir, M., Karaduman Er, I., Coşkun, A., Ateş, A., Acar, S.: The effect of deposition time on the structural, morphological and H<sub>2</sub>S gas sensing properties of the V<sub>2</sub>O<sub>5</sub> nanostructures deposited by hydrothermal method. *J. Mater. Sci. Mater. Electron.* **30**, 12215–12223 (2019)

**Publisher's Note** Springer Nature remains neutral with regard to jurisdictional claims in published maps and institutional affiliations.

Springer Nature or its licensor (e.g. a society or other partner) holds exclusive rights to this article under a publishing agreement with the author(s) or other rightsholder(s); author self-archiving of the accepted manuscript version of this article is solely governed by the terms of such publishing agreement and applicable law.